ChemCatChem

Research Article
doi.org/10.1002/cctc.202400169

Chemistry Europe
European Chemical Societies Publishing

www.chemcatchem.org

Metal Phosphide Nanoparticles Generated via a Molecular Precursor Route for Hydrotreatment of Methyl Laurate

Diana García-Pérez,[a] M. Consuelo Álvarez-Galván,*[a] M. Carmen Capel-Sánchez,[a] José M. Campos-Martín,*[a] and Susan E. Habas[b]

Transition metal phosphide nanoparticles supported on silica were used as catalysts to investigate the hydrodeoxygenation of methyl laurate (used as a model compound for vegetable oils). Ni_2P, Ni_1Mo_1P, and $Ni_{1.6}Mo_{0.4}P$ were synthesized using a molecular precursor route. The nanoparticles were added to the silica support without any changes in their structure or particle size. As a reference and for comparison, MoP/SiO_2 was also prepared by the phosphite method. The prepared catalysts were characterized by X-ray diffraction, X-ray photoelectron spectroscopy, transmission electron microscopy, and chemical analysis. A higher conversion is reached with the MoP/SiO_2 monometallic catalyst, close to that with Ni_1Mo_1P/SiO_2. However, this observation is misleading because the differences in dispersion obscure the result that the intrinsic activity (turnover frequency) of the bimetallic catalyst, prepared by a molecular precursor route, is significantly higher than that of the monometallic catalyst, prepared by the phosphite route, revealing a synergistic effect on the catalytic activity due to the formation of the bimetallic phosphide.

1. Introduction

Nowadays there is huge interest in resources for alternative and renewable energy such as biomass since the current environmental concerns regarding the greenhouse effect and climate change, the increasing demand for energy associated with the dwindling of fossil reserves, and the restrictive emissions on the environment.[1–3] Fuels derived from biomass have some advantages compared to traditional fuels, such as decreased emissions of greenhouse gases, regional production, and advantageous cost-effective use.[4] In particular, the use of vegetable oils and fats (waste residues) represents a promising alternative to producing jet fuels, and platform chemicals from renewable resources.[5]

The expectation for the coming decades is that liquid hydrocarbons will continue to be necessary as transportation fuels, especially in aviation, although other renewable energies are also growing in importance to meet the energy demand.[1] Hydrotreatment has become attractive technique for conversion of oil or fats into hydrocarbon-based fuels.[4,6] The quality of these hydrocarbon-based fuels obtained from hydrotreated vegetable oils (HVOs) is undoubtedly higher than that of biodiesel fuels obtained from methyl esters. Reducing the oxygen content is a critical requirement to produce a liquid product with the characteristics of a drop-in fuel.[7] Hydrotreatment of vegetable oils reduces NO_x and particulate matter emissions. The obtained fuels have good cold properties and are stable and highly compatible with engine oils. HVOs are hydrocarbons with a straight chain, a high cetane number and no aromatic, oxygen, or sulfur content.[6,8]

Regarding the catalysts used in the hydrotreatment process, several catalyst compositions can be used (sulfides, phosphides, noble metals).[9] This article is focused on transition metal phosphide (TMP) nanoparticles (NPs). Depending on the catalysts used, hydrotreatment undergoes through hydrodeoxygenation or decarbonylation/decarboxylation pathways to yield *n*-alkanes.[10] Transition metal phosphides are very interesting, showing a high activity and an electronic structure, stability, and resistance to water, similar to those of noble metals.[4] In the case of transition metal phosphide (TMP) nanoparticles (NPs) as catalysts, improvements in the synthesis of NPs have allowed control of the size, shape, and composition of the NPs.[11] During NP synthesis, organic ligands are added to control growth and stabilize these NPs before dispersing them on a high surface area support. These catalysts show excellent activity for hydrogenation reactions, such as hydrodesulfurization, hydrodenitrogenation, and hydrodeoxygenation.[12–14]

Overall, transition metal phosphide NPs have become a versatile catalytic material whose properties can be tuned to modulate the catalytic performance.[15] Traditional methods for making TMP nanomaterials could entail difficulties to control the particle morphology, phase impurities, and excess phosphorus species as they depend on high temperature (> 500 °C) programmed reduction of metal and phosphorus

[a] D. García-Pérez, M. C. Álvarez-Galván, M. C. Capel-Sánchez, J. M. Campos-Martín
Instituto de Catálisis y Petroleoquímica (CSIC), c/Marie Curie, 2, 28049 Madrid, Spain
E-mail: c.alvarez@icp.csic.es
jm.campos@csic.es

[b] S. E. Habas
National Renewable Energy Laboratory, Catalytic Carbon Transformation & Scale-up Center, Golden, 80401 Colorado, USA

Supporting information for this article is available on the WWW under https://doi.org/10.1002/cctc.202400169

precursors.[16,17] To resolve these problems, solution-synthesis methods[18–22] such as those that employ metal-phosphine compounds with adjustable decomposition temperatures,[11,15,23,24] have made it possible to create binary TMP NPs with uniform structural characteristics. However, ternary phases are more difficult to synthesize due to the differences in reactivity between the two metal precursors, which can lead to phase segregation and morphological inhomogeneities.[16] In this context, some advances have been done by Brock *et al* and Habas *et al*.[25] This last contribution consists of a solution synthesis to incorporate a second metal into the binary Ni_2P structure using molecular precursors and low temperatures. In that way, ternary TMP NPs have been prepared without changing the parent Ni_2P NPs' morphology or crystal phase, meaning with controlled composition.[17] Here, we utilize this approach to incorporate Mo into a parent Ni_2P catalyst. To the best of our knowledge, no other articles have been published for the case of hydrotreatment reaction using metal and bimetallic phosphide nanoparticles prepared by a molecular precursor route. Here, we present an original and practical application of metal phosphide nanoparticles used as catalysts.

The aim of this study is to test the activity of silica-supported metal phosphide NP catalysts prepared by the above route in the hydrodeoxygenation of methyl laurate (a model compound for vegetable oils) to yield green liquid fuels. Ni_2P, Ni_1Mo_1P and $Ni_{1.6}Mo_{0.4}P$ were synthesized as metal phosphide NPs and deposited onto a silica support to obtain the following catalysts: Ni_2P/SiO_2, Ni_1Mo_1P/SiO_2 and $Ni_{1.6}Mo_{0.4}P/SiO_2$. For comparison and as a reference, the MoP/SiO_2 catalyst was also prepared by the phosphite method.[4] The activity was related to the physicochemical characterization results to find the properties that play an important role in the catalytic activity.

Experimental

Chemicals

The following compounds were used as precursors: oleylamine (OAm, 70%), 1-octadecene (ODE, 90%), triphenylphosphine (PPh_3, 99%) and phosphorous acid (H_3PO_3, Sigma–Aldrich, 99%) purchased from Sigma–Aldrich. The $Ni(PPh_3)_2(CO)_2$ complex was purchased from Strem Chemicals, and $(NH_4)_6Mo_7O_{24}\cdot 4H_2O$ (99%) was purchased from Merck. Concerning the support, commercial pelletized silica was acquired from Saint Gobain-NORPRO (1.5 mm cylindrical pellets, SS 61138).

Catalyst Preparation

Synthesis of Nickel Phosphide (Ni_2P) NPs

These NPs were prepared following the procedure described in literature.[12,26] This procedure mainly consists of the synthesis *in situ* in the laboratory of the NPs, and it is in detailed described in the supplementary information. After the synthesis, the NPs were suspended in chloroform and added to the silica support by the incipient wetness impregnation method to get the Ni_2P/SiO_2 catalyst.

Synthesis of Nickel and Molybdenum Phosphide ($Ni_{1.6}Mo_{0.4}P$ and Ni_1Mo_1P) NPs

These NPs were prepared following the procedure described in.[25] After synthesis, the NPs were suspended in chloroform and added to the silica support to form the $Ni_{1.6}Mo_{0.4}P/SiO_2$ and Ni_1Mo_1P/SiO_2 catalysts. It is highlighted that these bimetallic phosphide catalysts in particular, have not been prepared before. This adds a new an original experimental procedure in this article.

Synthesis of Molybdenum Phosphide (MoP/SiO_2)

This catalyst was prepared following the method described in.[4] This method of preparation is called the temperature programmed reduction method.[26]

Catalyst Characterization Methods

The crystalline phases of the catalysts were studied with powder X-ray diffraction (XRD) analysis. The morphology of the catalysts was analyzed by transmission electron microscopy (TEM). X-ray photoelectron spectroscopy (XPS) measurements were applied to study the metal surface dispersion and oxidation states of the catalysts. Elemental analysis via ICP–OES was used to confirm the metal loadings.

Catalytic Activity Tests

Hydrotreatment of methyl laurate was used to evaluate the catalysts in a trickle-bed mode reactor. Two grams of inert silica support was used to dilute 1 gram of the reduced/passivated catalysts. The catalysts were reactivated by *in situ* reduction in flowing H_2 (200 mL_N/min) at 450 °C and atmospheric pressure for 3.5 h before catalytic evaluation. Catalytic conversion of methyl laurate was performed at 300 or 350 °C and 2.0 MPa with a liquid flow of 0.1 or 0.05 $mL\cdot min^{-1}$ and H_2 flow of 230 $mL_N\cdot min^{-1}$.

All detailed information about the catalyst preparation methods, catalyst characterization methods and catalytic activity tests is included in the supplementary information.

2. Results and Discussion

Inductively coupled plasma-optical emission spectroscopy (ICP-OES) was used to confirm the chemical compositions of the catalysts, as shown in Table 1. It is observed that the chemical composition results are very similar to the nominal values.

X-ray diffraction was applied to study the crystalline phases of the catalysts. Figure 1A shows the XRD patterns of the unsupported metal phosphide NPs. The diffraction peaks of the monometallic sample are assigned to hexagonal Ni_2P (PDF 00-003-0953): 40.8° (111), 44.4° (201), 47.3° (210), 54.4° (300), 66.4° (310), 72.8° (311), 74,9° (400), 80.5° (401) and 88.6° (321). For bimetallic catalysts, a transformation in the phase occurred due to the presence of Mo. The diffraction peaks correspond to hexagonal NiMoP (PDF 00-031-0873),

Research Article
doi.org/10.1002/cctc.202400169
Chemistry Europe
European Chemical Societies Publishing

Table 1. Chemical composition of the catalysts determined by ICP–OES.

Catalysts	Ni (wt.%) nominal	Mo (wt.%) nominal	Ni (wt.%) experimental	Mo (wt.%) experimental
Ni_2P/SiO_2	3.6	–	3.1	–
$Ni_{1.6}Mo_{0.4}P/SiO_2$	3.6	1.5	3.3	1.2
Ni_1Mo_1P/SiO_2	3.5	5.7	3.4	5.2
MoP/SiO_2	–	5.7	–	5.4

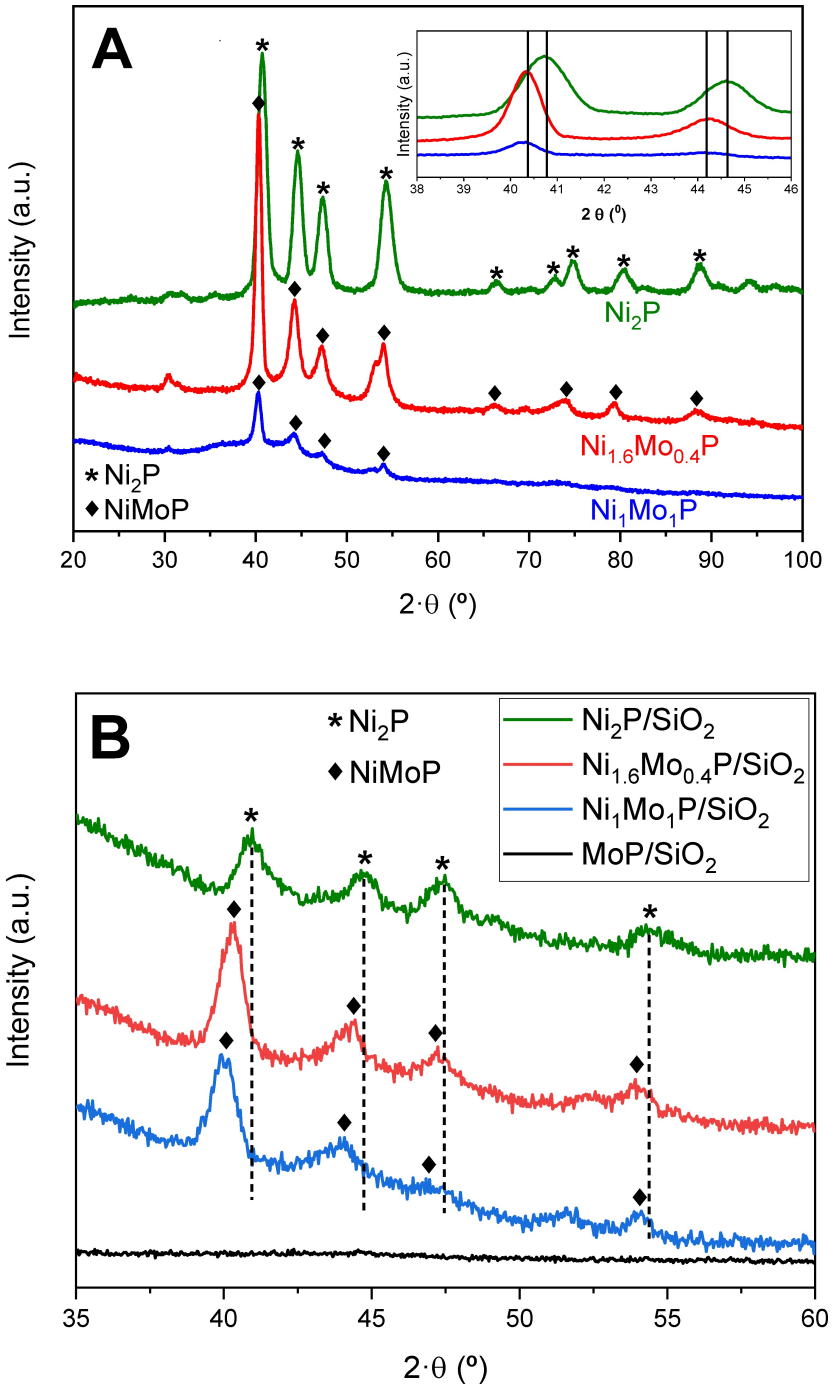

Figure 1. XRD diffractograms of the (A) metal phosphide NPs and (B) catalysts.

with the diffraction peaks at 40.3°, 44.2°, 47.3°, 54.1°, 66.2°, 74,0°, 79.5° and 88.6° attributed to the (111), (201), (210), (300), (310), (400), (401) and (321) crystal planes, respectively. For the Ni:Mo ratio of 0.25, the peaks are less intense and are broadened and shifted to lower angles with respect to Ni_2P (Figure 1A inset), which is attributed to lattice expansion because the smaller Ni atoms were substituted by larger Mo atoms.[25] For the Ni:Mo ratio of 1, the crystallinity is clearly decreased, but the main peaks are maintained with lower intensity, as is the shift of the peaks. Figure 1B shows the XRD patterns of the monometallic and bimetallic catalysts supported on silica. All the catalysts have a broad diffraction band (not shown) located at $2\theta = 20–30°$ due to amorphous silica. Related to the phosphide, the same peaks are observed in the catalysts and in the unsupported NPs, confirming that Ni_2P, $Ni_{1.6}Mo_{0.4}P$ and Ni_1Mo_1P crystallites are also found on the silica support.[27] In terms of calculated particle size by Scherrer equation, the obtained values (Table 2) are very similar in both, unsupported and supported metal phosphides NPs. The small difference in the case of Ni_1Mo_1P could be due to an excess ligand present for the unsupported NPs, diluting the overall signal and giving an amorphous background. In conclusion, the structure of the crystalline phase's changes with the incorporation of Mo and are characteristic of bimetallic metal phosphide NPs. Adding this much Mo led to a more amorphous composition as Mo–P NPs can be amorphous according to the literature.[4,10]

In addition, the average crystallite sizes of metal phosphide NPs were determined using the Scherrer equation (Table 2). As expected, these sizes are maintained when the nanoparticles are unsupported or supported on silica.

Figure 2 depicts TEM images and the particle size distributions of the metal phosphide NPs and MoP/SiO_2 catalyst. Figure 1S depicts TEM images and the particle size distributions of the reduced/passivated NP catalysts (NPs supported on silica). The spherical NPs observed in TEM micrographs for all the catalysts are assigned to metal phosphides, as observed in other studies.[25,28,29] The metal phosphide nanoparticles range in size from 9.5 in Ni_2P/SiO_2 to 12.4 nm in $Ni_{1.6}Mo_{0.4}P/SiO_2$ and 14.4 nm in Ni_1Mo_1P/SiO_2, whereas the analysis of MoP/SiO_2 gives a size of 2.6 nm, showing a much higher dispersion of particles than the other catalysts.[30,31] The increase in the size from the Ni_2P/SiO_2 to $Ni_{1.6}Mo_{0.4}P/SiO_2$ and Ni_1Mo_1P/SiO_2 catalysts is due to the formation of bimetallic phosphides after the incorporation of larger Mo atoms.[25]

The high-resolution micrographs were used to measure the distance between the planes in agreement with the International Centre for Diffraction Data (ICDD). Figure 2 A-1 shows a Ni_2P nanoparticle with a d-spacing of 2.19 Å assigned to the (001) crystallographic plane of Ni_2P (PDF 00-003-0953). Figure 2 B-1 shows a $Ni_{1.6}Mo_{0.4}P$ nanoparticle with a d-spacing of 2.22 Å assigned to the (111) crystallographic plane of NiMoP (PDF 00-031-0873). Figure 2 C-1 shows a Ni_1Mo_1P nanoparticle with a d-spacing of 2.24 Å assigned to the (111) crystallographic plane of NiMoP (PDF 00-031-0873). These measurements confirm the existence of the corresponding monometallic and bimetallic phases.

Table 2 shows the particle sizes measured with TEM and XRD. In general, the crystallite sizes are close to the average size of metal phosphide NPs obtained with TEM micrographs. This fact reveals that the molecular precursor route used for the synthesis produces monocrystalline metal phosphide NPs. The NP sizes were also maintained after impregnation of the active phase into the silica support. The particle size of MoP/SiO_2 is clearly smaller than that of the other samples and was only measured by TEM because no diffraction peaks were detected for this sample.

XPS was applied to analyze the surface chemical state of the reduced/passivated catalysts. Figure 3 compiles XPS spectra of the catalysts, and Table 3 shows the core-electron binding energies (eV) (Si 2p, Mo 3d, Ni 2p and P 2p core levels) and the corresponding surface atomic ratios.

The binding energies (BEs) were referenced to the Si 2p signal at 103.3 eV to correct for charging effects. In the P 2p spectra of all the catalysts, there is a component at approximately 125.5 eV attributed to $P^{\delta-}$, which is present in the phosphide phase. The XPS spectrum of MoP/SiO_2 in the Mo 3d region shows the spin-orbital splitting of d energy levels, with the presence of double peaks contribution of $3d_{5/2}$ and $3d_{3/2}$. The discussion of the present Mo species will be done taking in account only $3d_{5/2}$ peaks, because the same effect is present for $3d_{3/2}$. The monometallic sample shows the presence of two components, a peak at 228 eV attributed to Mo^0 species, and a second contribution at 230.2 eV characteristic of MoP species. For the bimetallic catalysts, we detected two species too, but shifted to lower BE as the ratio Ni/Mo contents is higher, Ni_1Mo_1P/SiO_2 (226.5, and 229.2 eV respectively) and $Ni_{1.6}Mo_{0.4}P/SiO_2$, (225.8 and 228.6 eV) where the intensity of the peaks is proportional to the amount of Mo on the catalysts.[4,10,32,33] This shift in the BE clearly indicates a strong interaction between Ni and Mo in the

Table 2. Particle sizes obtained by XRD and TEM.

Catalysts	TEM NPs (nm)	TEM SiO_2 (nm)	XRD NP crystallite size (nm)	XRD SiO_2 crystallite size (nm)	Crystal phase	PDF card	2θ (°)
Ni_2P/SiO_2	8.7	9.5	9.6	9.8	Ni_2P	00-003-0953	40.9
$Ni_{1.6}Mo_{0.4}P/SiO_2$	11.7	12.4	12.3	12.2	NiMoP	00-031-0873	40.3
Ni_1Mo_1P/SiO_2	14.3	14.4	14.1	13.0	NiMoP	00-031-0873	40.1
MoP/SiO_2	–	2.6	–	–	–	–	–

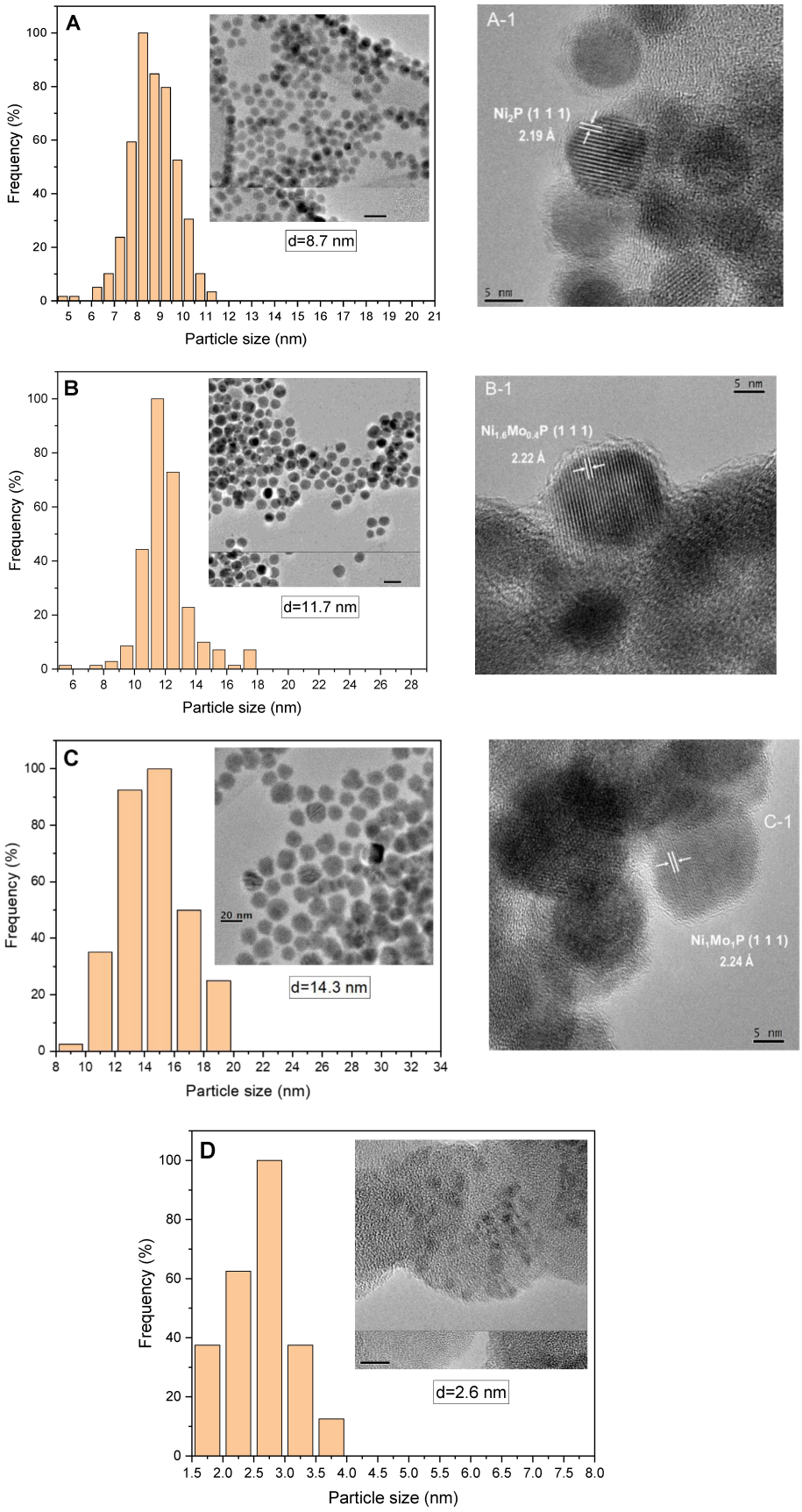

Figure 2. TEM images of the (A) Ni_2P, (B) Ni_1Mo_1P, (C) $Ni_{1.6}Mo_{0.4}P$ and (D) MoP/SiO_2 catalysts.

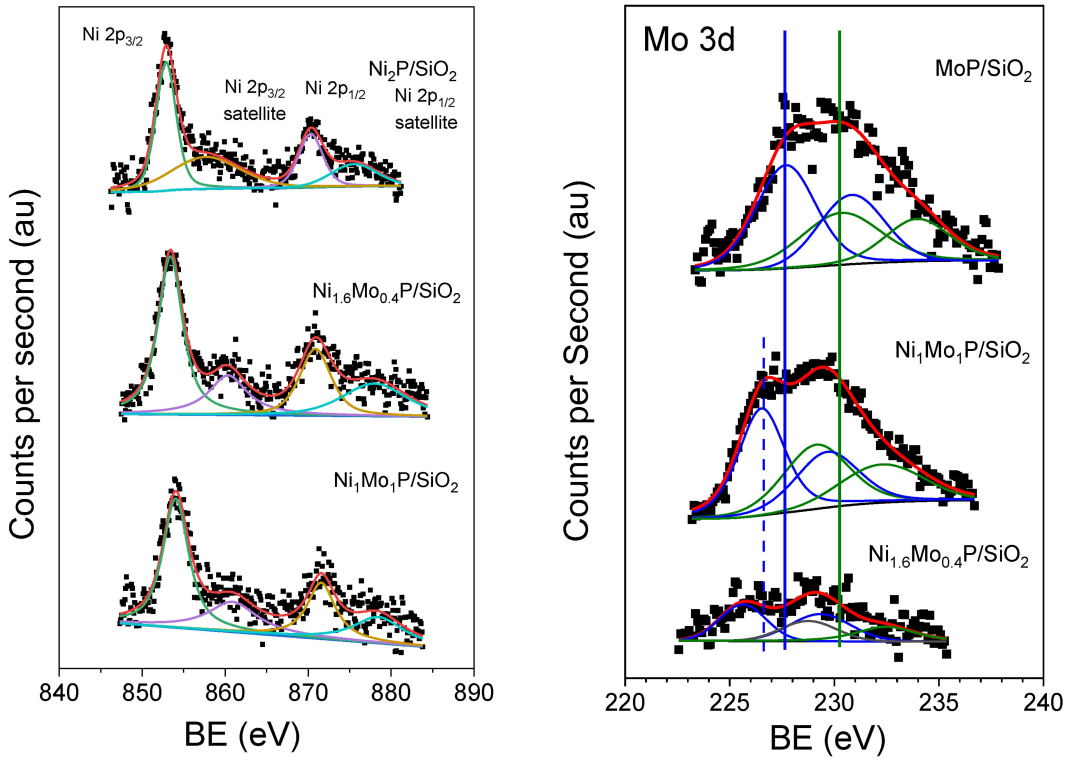

Figure 3. XPS spectra of the Ni 2p region and Mo 3d region for the catalysts.

Table 3. Spectral parameters obtained by XPS for the reduced/passivated catalysts.

Catalysts	P2p	Ni2p$_{3/2}$	Mo3d$_{5/2}$	P/Si (at)	Mo/P (at)	Ni/P (at)	Mo/Si (at)	Ni/Si (at)	(Mo/Si)xps/ (Mo/Si)nom	(Ni/Si)xps/ (Ni/Si)nom
Ni_2P/SiO_2	125.6	853.0	–	0.067	–	0.126	–	0.0084	–	0.00835
$Ni_{1.6}Mo_{0.4}P/SiO_2$	125.3	853.5	225.8 229.3	0.065	0.076	0.176	0.005	0.0115	0.02078	0.01150
Ni_1Mo_1P/SiO_2	125.2	854.1	226.5 229.2	0.064	0.259	0.123	0.017	0.0079	0.0172	0.00812
MoP/SiO_2	125.4	-	228.0 230.2	0.060	0.162	–	0.010	–	0.1	–

bimetallic samples that confirms the formation of bimetallic phosphides.

Ni 2p region showed the spin-orbital splitting with doublet peaks ($2p_{3/2}$ and $2p_{1/2}$). We detected only a nickel specie in all samples analyzed, Ni_2P/SiO_2, $Ni_{1.6}Mo_{0.4}P/SiO_2$ and Ni_1Mo_1P/SiO_2 catalysts, with the presence of the typical satellite peak present in Ni 2p region. The monometallic sample shows a peak 853 eV is due to $Ni^{\delta+}$ in phosphides.[34–36] The bimetallic samples showed also peak but shifted to higher BE, 853.5 eV for $Ni_{1.6}Mo_{0.4}P/SiO_2$ and 854.1 eV for Ni_1Mo_1P/SiO_2. These results confirm the interaction between Ni and Mo due to the formation of bimetallic phosphides.

If we compare the P/Si ratios of all the catalysts, very similar ratios are obtained, meaning that M/P or M/Si comparisons make sense to obtain an approach for surface metal dispersion. For comparison of the metal phosphide dispersions obtained for each catalyst, the ratio (M/Si)xps/(M/Si)nominal was calculated. In the case of molybdenum, the following trend is found: $MoP/SiO_2 > Ni_{1.6}Mo_{0.4}P/SiO_2 \approx Ni_1Mo_1P/SiO_2$. This confirms the fact that MoP achieves a higher dispersion. For nickel, the trend is $Ni_{1.6}Mo_{0.4}P/SiO_2 > Ni_2P/SiO_2 \approx Ni_1Mo_1P/SiO_2$.

In summary, after studying the characterization results of the catalysts with the different techniques discussed (X-ray diffraction, ICP–OES, TEM and XPS), we can conclude that bimetallic phases were successfully formed.

To evaluate the catalytic activity of the materials, the four monometallic and bimetallic catalysts were tested in the hydrodeoxygenation reaction of methyl laurate to hydrocarbons. A summary of the activity test results is presented in Figure 4.

Ni_2P/SiO_2 and $Ni_{1.6}Mo_{0.4}P/SiO_2$ show very low activity in the HDO of methyl laurate at either 300 or 350 °C. However,

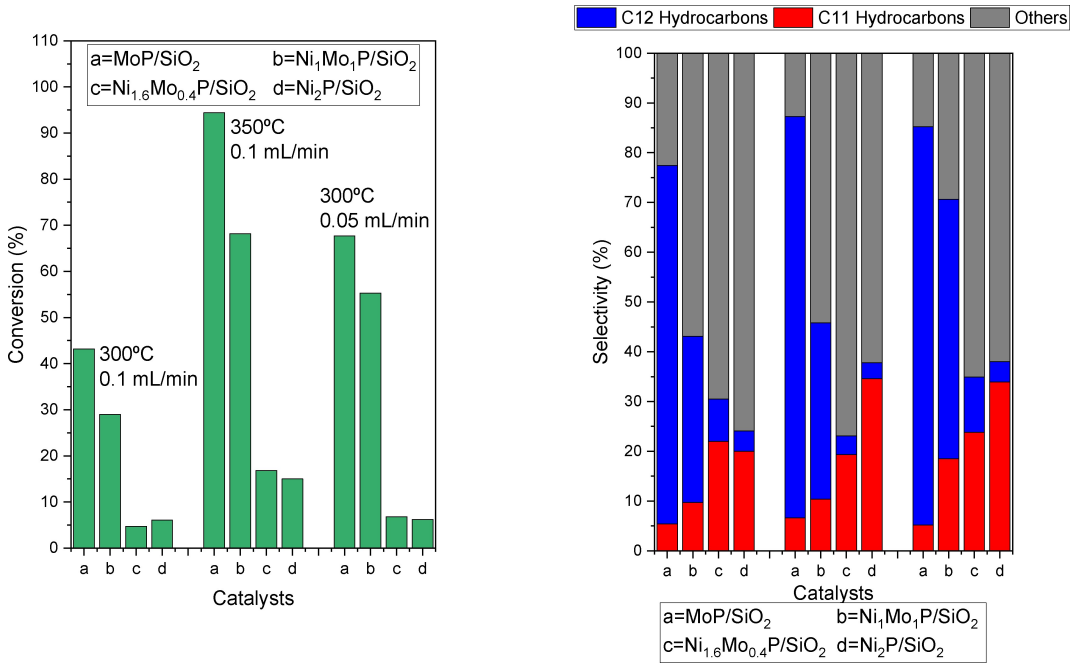

Figure 4. Conversion and selectivity for hydrodeoxygenation of methyl laurate (300–350 °C, 2.0 MPa and liquid flow of 0.05–0.1 mL/min).

MoP and Ni_1Mo_1P are active catalysts at both temperatures, showing a higher activity than the catalysts with a low proportion of or no Mo. The catalysts are stable only at 300 °C. Upon increasing the temperature from 300 to 350 °C, all the catalysts show a higher initial activity,[28,34] but this activity decreases after the beginning of the reaction.[37] The conversion results shown at 350 °C correspond to the initial conversion value obtained, as the deactivation makes it impossible to correctly calculate the average value (Figure 2S).

A decrease of the liquid flow yields a higher activity for all the catalysts because a low liquid flow corresponds to a high contact time between the liquid and the catalyst.[8] However, the conversion for Ni_2P/SiO_2 and $Ni_1Mo_{0.4}P/SiO_2$ is still too low to consider them as suitable catalysts for this reaction.

In terms of selectivity, hydrocarbons are the main obtained products, but oxygenated compounds (mainly lauric acid or dodecanoic acid and lauryl alcohol or dodecanol) are also produced in minor proportions, named as "others" in Figure 4. The obtained selectivity shows that for the MoP/SiO_2 catalyst, the main products are C_{12} hydrocarbons, while for Ni_2P/SiO_2, the main products are C_{11} hydrocarbons. These differences between the C_{11} and C_{12} proportions indicate that the Mo-based catalyst favors a hydrogenation pathway and that the Ni-based catalyst favors a decarbonylation/decarboxylation pathway with oxygen elimination.[4,10] In the catalyst with equimolar amounts of Ni and Mo, the hydrogenation pathway is the main route, and C_{12} hydrocarbons are the primary obtained products; however, a higher proportion of C_{11} is detected with respect to the molybdenum only counterpart.

An increase of the reaction temperature produces an enhancement of the hydrocarbon selectivity with a decrease in the oxygenated compounds. This effect is related to an increase in the conversion because at higher temperatures, the oxygenated intermediates are consumed, and the final product formation is increased. No changes in the C_{12}/C_{11} hydrocarbon ratio are detected with the temperature change; C_{12} hydrocarbons are the main products for the catalysts with a higher Mo content, and C_{11} hydrocarbons are the main products for the catalysts with a higher Ni content.

The turnover frequencies (TOFs) were calculated with the converted moles of methyl laurate in the steady state and the metal dispersions obtained by TEM to determine the activity per mol of surface metal phosphide.[38,39] All detailed calculation is included in the supplementary information. The TOF results indicate that the intrinsic activity shows the following trend: $Ni_1Mo_1P > MoP > Ni_{1.6}Mo_{0.4}P \sim Ni_2P$ (Table 4). These results show an increase in the TOF for Ni_1Mo_1P/SiO_2 (6.9 min^{-1}), prepared by the molecular precursor route, with respect to MoP/SiO_2 (2.6 min^{-1}), prepared by the phosphite route. The formation of a bimetallic phosphide, sharing the same crystal lattice, enhances the intrinsic activity of the phosphide catalyst. These results are not reflected in the conversion values because of the differences in the dispersion of the Mo monometallic catalyst (MoP/SiO_2) and the bimetallic catalyst (Ni_1Mo_1P/SiO_2). Future studies will be focused on the synthesis of bimetallic molybdenum metal phosphide NPs with a higher dispersion, using the molecular precursor route, which could maximize the conversion results.

A few articles are using bimetallic phosphides catalysts in particular, synthesized by the phosphite and phosphate

Table 4. Study of the temperature and liquid flow conditions of the studied catalysts and comparison with other published studies in the hydrodeoxygenation of methyl laurate.

Catalysts	T (°C)	P (MPa)	Liquid flow (mL/min)	Conv. (%)	HC C_{12}	HC C_{11}	HC C_{6-10}	Oxygenated compounds	TOF (min^{-1})	Reference
Ni_2P/SiO_2	300	2.0	0.1	6.1	4.1	20.0	15.9	10.5	1.9	This work
$Ni_1Mo_{0.4}P/SiO_2$	300	2.0	0.1	4.7	8.5	22.0	6.6	19.1	1.6	This work
Ni_1Mo_1P/SiO_2	300	2.0	0.1	29.0	33.4	9.7	2.6	39.7	6.9	This work
MoP/SiO_2	300	2.0	0.1	43.2	72.0	5.4	3.5	8.7	2.6	This work
Ni_2P/SiO_2	300	2.0	0.05	6.2	4.1	33.9	8.8	11.2	1.0	This work
$Ni_1Mo_{0.4}P/SiO_2$	300	2.0	0.05	6.8	11.1	23.8	4.3	22.0	1.1	This work
Ni_1Mo_1P/SiO_2	300	2.0	0.05	55.3	52.1	18.5	1.0	17.5	6.6	This work
MoP/SiO_2	300	2.0	0.05	67.7	80.0	5.2	2.0	3.9	2.0	This work
$Ni_{10}MoP/SiO_2$	290	3.0	–	~77	~87		–	–	5.4	[32]
$MoNiP_2/SiO_2$-C500	300	-	–	~80	~78		–	~5	10.2	[40]
Ni/γ-Al_2O_3	300	2.0	–	~76	~3	~65	~8	~10	-	[41]
NiMo/HBeta(13)	300	0.4	–	~80	~27	~43	~5	~2	-	[42]
Ni/ZrO_2/γ-Al_2O_3	300	2.0	–	~23	~3	~50	~2	~38	-	[43]
Ni/ZSM-5 (8NiZ5–18)	280	2.0	–	~83	~78		–	–	-	[44]
Ni/SiO_2–TiO_2	300	2.5	–	~100	~98	~2	–	-	2.6	[45]
4Ni/Beta	280	2.0	–	~77	~43		~	~8	1.3	[46]

methods, in the hydrotreatment of methyl laurate and those can also be compared to our present work. Z. Nie *et al.* studied the effect of Ni and on performance of bifunctional MoP/SiO_2 for hydroconversion of methyl laurate. They prepared, among others, the $Mo_{10}NiP$ catalyst and obtained conversions of methyl laurate around 80% and selectivity to C_{11+12} nearly 90% at 280 °C.[32]

Zhengyi Pan *et al.* studied SiO_2-supported Ni–Mo bimetallic phosphides (Mo/Ni molar ratio was 1.0) prepared by the phosphate method in the hydrodeoxygenation of methyl laurate. At 300 °C depending on the calcination temperature used, $MoNiP_2/SiO_2$ catalyst showed a conversion between 65–80% and a variable selectivity for $C_{11}+C_{12}$ (45–80%) for methyl laurate compound.[40]

The hydrotreatment of methyl laurate with similar catalysts has been previously investigated. Here in Table 4, we report some studies at the most similar conditions than in our reactions to compare the results, however, the comparisons are difficult due to the different support and synthesis procedures. Several articles are studying the hydrotreatment of methyl laurate using alumina and zeolites as supports and Ni or NiMo as active phases. For example, a study with NiMo/HBeta(13) catalyst[42] has reported a conversion of methyl laurate around 80% and selectivity to C_{12+11} around 70%. Another study with Ni–Mo/SiO_2–TiO_2 catalyst[45] showed a conversion of methyl laurate around 100% and selectivity to C_{12} around 98%.

The main information is related with the use of nickel-based catalysts, where the TOF values are similar to our monometallic Ni_2P/SiO_2 (see entries 1, 5, 15, and 16 of Table 4), and the bimetallic Ni–Mo phosphides (entries 9 and 10 of Table 4) have a TOF of the same order of our experiments. In consequence, we can assume that the results of the comparison of monometallic and bimetallic phosphides presented in this study, using the same preparation method and support, will help the understanding of this phenomenon. The increase in the TOF value found in our work for hydrotreatment of methyl laurate using Ni_1Mo_1P/SiO_2 catalyst, prepared by a molecular precursor method, with respect to the monometallic MoP/SiO_2, makes this catalyst synthesis method very promising.

3. Conclusions

Three different catalysts based on metal phosphide NPs supported on silica (Ni_2P/SiO_2, $Ni_{1.6}Mo_{0.4}P/SiO_2$ and Ni_1Mo_1P/SiO_2) were successfully prepared by a molecular precursor route. For comparison, another catalyst (MoP/SiO_2) was also prepared by the phosphite method. The formation of bimetallic phosphides was confirmed by the shift of diffraction peaks to lower angles with respect to Ni_2P, attributed to lattice expansion because the Ni atoms, which are smaller, were substituted by Mo atoms, which are larger. This observation was confirmed by high-resolution TEM micrographs that support this expansion, and the shift of binding energies detected by XPS.

The incorporation of the phosphide nanoparticles into the silica support does not change the particle size or other characteristics of the prepared nanoparticles.

The characterization of the different metal phosphide catalysts indicates that the metal dispersion achieved on the silica support is higher for the MoP/SiO_2 monometallic catalyst and lower for the Ni_2P/SiO_2, $Ni_{1.6}Mo_{0.4}P/SiO_2$ and

Ni_1Mo_1P/SiO_2 catalysts due to the differences in the preparation methods.

The catalytic activity reveals that catalysts with a high proportion of Mo (MoP/SiO_2 and Ni_1Mo_1P/SiO_2) favor the hydrogenation route, producing mostly C_{12} hydrocarbons, whereas catalysts with a high proportion of Ni (Ni_2P/SiO_2 and $Ni_{1.6}Mo_{0.4}P/SiO_2$) favor the decarbonylation/decarboxylation route, yielding more C_{11} hydrocarbons.

A higher conversion is reached with the MoP/SiO_2 monometallic catalyst, close to that with Ni_1Mo_1P/SiO_2. However, this observation is misleading because the differences in dispersion hide the result that the intrinsic activity (TOF) of the bimetallic catalyst is much higher than that of the monometallic catalyst, revealing a synergistic effect on the catalytic activity due to the formation of the bimetallic phosphide.

Acknowledgements

The support of MICIN/AEI (Spain) through project ENE2016-74889-C4-3-R is acknowledged. DGP acknowledges MICIN/AEI for her contract (BES-2017-079679) (Spain). This research has been developed within the CSIC Interdisciplinary Thematic Platform (PTI+) Transición Energética Sostenible+ (PTI-TRANSENER+) as part of the CSIC program for the Spanish Recovery, Transformation and Resilience Plan funded by the Recovery and Resilience Facility of the European Union, established by Regulation (EU) 2020/2094.

This work was authored in part by the National Renewable Energy Laboratory, operated by Alliance for Sustainable Energy, LLC, for the U.S. Department of Energy (DOE) under Contract No. DE-AC36-08GO28308.

The views expressed in the article do not necessarily represent the views of the DOE or the U.S. Government. The U.S. Government retains and the publisher, by accepting the article for publication, acknowledges that the U.S. Government retains a nonexclusive, paid-up, irrevocable, worldwide license to publish or reproduce the published form of this work, or allow others to do so, for U.S. Government purposes.

Conflict of Interests

The authors declare no conflict of interest.

Data Availability Statement

The data that support the findings of this study are available from the corresponding author upon reasonable request.

Keywords: Metal phosphide nanoparticles (NPs) · Green liquid fuels · Hydrotreatment · Methyl laurate · Vegetable oils or fats

[1] A. E. Coumans, E. J. M. M. Hensen, *Appl. Catal. B Environ.* **2017**, *201*, 290–301, doi: https://doi.org/10.1016/j.apcatb.2016.08.036.
[2] V. L. Dagle, et al., *ACS Catal.* **2020**, *10*(18), 10602–10613, doi: 10.1021/acscatal.0c02235.
[3] S. Izaddoust, et al., *Fuel* **2022**, *325*, 124765, doi: 10.1016/J.FUEL.2022.124765.
[4] M. C. Alvarez-Galvan, G. Blanco-Brieva, M. Capel-Sanchez, S. Morales-delaRosa, J. M. Campos-Martin, J. L. G. G. Fierro, *Catal. Today* **2018**, *302*, 242–249, doi: https://doi.org/10.1016/j.cattod.2017.03.031.
[5] P. Mäki-Arvela, M. Martínez-Klimov, D. Y. Murzin, *Fuel* **2021**, *306*, 121673, doi: 10.1016/J.FUEL.2021.121673.
[6] M. Žula, M. Grilc, B. Likozar, *Chem. Eng. J.* **2022**, *444*, 136564, doi: 10.1016/J.CEJ.2022.136564.
[7] D. A. Ruddy, C. O. Us, F. R. Gabriel, C. O. Us, "(12) United States Patent," 2, **2019**.
[8] M. C. Alvarez-Galvan, J. M. Campos-Martin, J. L. G. Fierro, *Catalysts* **2019**, *9*(3), 293, doi: 10.3390/catal9030293.
[9] P. Kumar, D. Verma, M. G. Sibi, P. Butolia, S. K. Maity, *Hydrodeoxygenation of triglycerides for the production of green diesel: Role of heterogeneous catalysis*, Elsevier Inc., **2022**, 97-126, doi: 10.1016/B978-0-12-823306-1.00013-3.
[10] D. García-Pérez, et al., *Catal. Today* **2021**, *367*, 43–50, doi: 10.1016/j.cattod.2020.09.034.
[11] S. E. Habas, et al., *Chem. Mater.* **2015**, *27*(22), 7580–7592, doi: 10.1021/acs.chemmater.5b02140.
[12] R. Prins, M. E. Bussell, *Catal. Letters* **2012**, *142*(12), 1413–1436, doi: 10.1007/s10562-012-0929-7.
[13] P. Clark, *J. Catal.* **2003**, *218*(1), 78–87, doi: 10.1016/s0021-9517(03)00086-1.
[14] L. Mora-Tamez, G. Barim, C. Downes, E. M. Williamson, S. E. Habas, R. L. Brutchey, *Chem. Mater.* **2019**, *31*(5), 1552–1560, doi: 10.1021/acs.chemmater.8b04518.
[15] C. A. Downes, et al., *Electrocatalytic CO 2 Reduction over Cu 3 P Nanoparticles Generated via a Molecular Precursor Route*, *ACS Appl. Energy Mater.* **2020**, *3(11)*, 10435–10446 doi: 10.1021/acsaem.0c01360
[16] J. Kolny-Olesiak, *Zeitschrift fur Naturforsch. - Sect. A J. Phys. Sci.* **2019**, *74*(8), 709–719, doi: 10.1515/ZNA-2019-0133.
[17] Y. Shi, B. Zhang, *Chem. Soc. Rev.* **2016**, *45*(6), 1529–1541, doi: 10.1039/c5cs00434a.
[18] S. Carenco, D. Portehault, C. Boissière, N. Mézailles, C. Sanchez, *Chem. Rev.* **2013**, *113*(10), 7981–8065, doi: 10.1021/cr400020d.
[19] S. L. Brock, S. C. Perera, K. L. Stamm, *Chem. - A Eur. J.* **2004**, *10*(14), 3364–3371, doi: 10.1002/chem.200305775.
[20] A. E. Henkes, Y. Vasquez, R. E. Schaak, *J. Am. Chem. Soc.* **2007**, *129*(7), 1896–1897, doi: 10.1021/ja068502l.
[21] S. Carenco, et al., *Chem. Mater.* **2012**, *24*(21), 4134–4145, doi: 10.1021/CM3022243/SUPPL_FILE/CM3022243_SI_001.PDF.
[22] M. E. Mundy, D. Ung, N. L. Lai, E. P. Jahrman, G. T. Seidler, B. M. Cossairt, *Chem. Mater.* **2018**, *30*(15), 5373–5379, doi: 10.1021/ACS.CHEMMATER.8B02206/ASSET/IMAGES/LARGE/CM-2018-02206V_0005.JPEG.
[23] M. Sun, H. Liu, J. Qu, J. Li, *Adv. Energy Mater.* **2016**, *6*(13), 1600087, doi: 10.1002/aenm.201600087.
[24] S. H. Li, M. Y. Qi, Z. R. Tang, Y. J. Xu, *Chem. Soc. Rev.* **2021**, *50*(13), 7539–7586, doi: 10.1039/D1CS00323B.
[25] C. A. Downes, et al., *Chem. Mater.* **2022**, *34*(14), 6255–6267, doi: 10.1021/ACS.CHEMMATER.2C00085.
[26] J. A. Cecilia, A. Infantes-Molina, E. Rodríguez-Castellón, A. Jiménez-López, *J. Catal.* **2009**, *263*(1), 4–15, doi: 10.1016/j.jcat.2009.02.013.
[27] S. J. Sawhill, D. C. Phillips, M. E. Bussell, *J. Catal.* **2003**, *215*(2), 208–219, doi: 10.1016/S0021-9517(03)00018-6.
[28] Z. Pan, R. Wang, M. Li, Y. Chu, J. Chen, *J. Energy Chem.* **2015**, *24*(1), 77–86, doi: 10.1016/S2095-4956(15)60287-X.
[29] X. Lan, E. J. M. Hensen, T. Weber, *Catal. Today* **2017**, *292*, 121–132, doi: 10.1016/J.CATTOD.2016.12.040.
[30] A. Berenguer, et al., *Green Chem.* **2016**, *18*(7), 1938–1951, doi: 10.1039/c5gc02188j.
[31] H. Y. Zhao, D. Li, P. Bui, S. T. Oyama, *Appl. Catal. A Gen.* **2011**, *391*(1–2), 305–310, doi: 10.1016/j.apcata.2010.07.039.
[32] Z. Nie, Z. Zhang, J. Chen, *Appl. Surf. Sci.* **2017**, *420*, 511–522, doi: 10.1016/J.APSUSC.2017.05.173.
[33] K. Li, R. Wang, J. Chen, *Energy Fuels* **2011** *25*, 854–863, doi: 10.1021/ef101258j.
[34] J. Chen, H. Shi, L. Li, K. Li, *Appl. Catal. B Environ.* **2014**, *144*(0), 870–884, doi: https://doi.org/10.1016/j.apcatb.2013.08.026.

[35] A. Infantes-Molina, E. Gralberg, J. A. Cecilia, E. Finocchio, E. Rodríguez-Castellón, *Catal. Sci. Technol.* **2015**, *5*(6), 3403–3415, doi: 10.1039/C5CY00282F.
[36] P. Liu, Z. X. Zhang, S. W. Jun, Y. L. Zhu, Y. X. Li, *React. Kinet. Mech. Catal.* **2019**, *126*(1), 453–461, doi: 10.1007/s11144-018-1496-8.
[37] M. A. Golubeva, E. M. Zakharyan, A. L. Maximov, *Pet. Chem.* **2020**, *60*(10), 89–111, doi: 10.1134/S0965544120100047.
[38] G. Bergeret, P. Gallezot, "3.1.2 Particle Size and Dispersion Measurements" in *Handb. Heterog. Catal.*, Wiley-VCH Verlag GmbH & Co. KgaA, **2008**, pp. 738–765, doi: 10.1002/9783527610044.hetcat0038.
[39] A. R. J. Kucernak, V. N. Naranammalpuram Sundaram, *J. Mater. Chem. A* **2014**, *2*(41), 17435–17445, doi: 10.1039/c4ta03468f.
[40] Z. Y. Pan, R. J. Wang, M. F. Li, Y. Chu, J. X. Chen, *J. Energy Chem.* **2015**, *24*(1), 77–86, doi: 10.1016/s2095-4956(15)60287-x.
[41] S. Chen, G. Zhou, H. Xie, Z. Jiao, X. Zhang, *Appl. Catal. A, Gen.* **2019**, *569*, 35–44.
[42] H. Imai, et al., *Fuel Process. Technol.* **2020**, *197*, 106182, doi: 10.1016/j.fuproc.2019.106182.
[43] S. Chen, M. Leng, Z. Liao, J. Zeng, H. Xie, G. Zhou, *Ind. Crop. Prod.* **2024**, *211*, 118227, doi: 10.1016/j.indcrop.2024.118227.
[44] T. Wang, et al., *Ind. Eng. Chem. Res.* **2023**, *62*, 16513–16520, doi: 10.1021/acs.iecr.3c02328.
[45] L. Fu, et al., *Appl. Catal. A, Gen.* **2022**, *633*, 118475, doi: 10.1016/j.apcata.2021.118475.
[46] T. Wang, et al., *Fuel Process. Technol.* **2023**, *241*, 107602, doi: 10.1016/j.fuproc.2022.107602.

Manuscript received: January 27, 2024
Revised manuscript received: April 15, 2024
Accepted manuscript online: April 17, 2024
Version of record online: May 31, 2024